Compact Plasma Accelerator for Micro-propulsion Applications[*†]

John E. Foster
NASA Glenn Research Center
Cleveland, OH 44135 USA
216-433-6131
John.Foster@GRC.NASA.Gov
IEPC-01-221

There is a need for a low power, light-weight (compact), high specific impulse electric propulsion device to satisfy mission requirements for micro-satellite (1-20 kg) class missions. Satisfying these requirements entails addressing the general problem of generating a sufficiently dense plasma within a relatively small volume and then accelerating it. In the work presented here, the feasibility of utilizing a magnetic cusp to generate a dense plasma over small length scales of order 1 mm is investigated. This approach could potentially mitigate scaling issues associated with conventional ion thruster plasma containment schemes. Plume and discharge characteristics were documented using a Faraday probe and a retarding potential analyzer.

Nomenclature

A = Area of retarding potential analyzer collector
a = Channel radius
B = Magnetic field
$D_\perp$ = Cross-field electron diffusion coefficient
D_a = Field free electron diffusion coefficient
E = Electric Field
e = Elementary charge of an electron
m_T = Total Xenon flow rate
f(u_i) = Ion velocity distribution function
F = Thrust
$F_\parallel$ = Magnetic mirror force
g = Gravitational constant
I = Ion current
I_d = Discharge current
J_b = Ion beam current
k = Boltzmann's constant
l = Channel length
M = Mass of xenon

u_i = Ion velocity
N = Number of apertures
n_o = Neutral density
P_a = Arithmetic mean of P_1 and P_2
P_1 = Pressure in the channel
P_2 = Pressure in the vacuum vessel
Q = Flow potential
s = Displacement along B
V = Retarding potential analyzer voltage
V_f = Floating potential with respect to ground
V_s = Plasma potential with respect to ground
V_b = Ion energy
z = Axis of symmetry
g = Thrust loss correction factor
h = Gas viscosity
h_u = Propellant utilization efficiency
m = Magnetic moment
v = Electron-neutral collision frequency
s_i = Electron neutral ionization cross section
w = Electron cyclotron frequency

Introduction

There is a growing interest in the development of micro-spacecraft. The main benefit of these low mass

(1-20 kg) satellites is the associated launch cost savings.[1] A fleet of these small spacecraft can be used for endeavors such as particle and field mapping missions. Launching one or a fleet of small spacecraft to do the job of a larger conventional satellite is now possible with recent miniaturization advances in the micro-electromechanical systems (MEMS) and microelectronics.[1,2] In this respect sensors and probes can now be assembled in low volume packages that make up the micro-spacecraft. These micro-spacecraft will require a miniaturized propulsion system as well. The thrusters will be used for applications such as disturbance compensation (ex. Space Technology 7), position correction, general station-keeping, and primary propulsion for small probes. Propulsion, however, has lagged behind the rapid advances in miniaturization of other spacecraft components. This is particularly the case for micro-spacecraft requiring a high specific impulse propulsion option. Propulsion systems such as field emission plasma thrusters, pulsed plasma thrusters and colloid thrusters are fairly mature technologies that could potentially satisfy some of the micro-spacecraft requirements. Unfortunately, these systems tend to generate potentially contaminating plumes.[1] Generally speaking, inert gas ion accelerator systems are non-contaminating, high specific impulse options.[1] Presently, the state of the art in ion thruster technology is embodied in the NASA Solar Electric Propulsion Test and Applications Readiness (NSTAR) Deep Space 1 ion engine.[3,4] This 30 cm device, however, is far to large, volume- and mass-wise, to satisfy micro-propulsion requirements.

In an attempt to address the need for a low mass/volume and low power, high specific impulse option, a number of approaches are being investigated. These include the micro-ion thruster scheme under development at JPL.[5,6,7] In JPL approach, an ion thruster discharge chamber and grids would be fabricated via MEMS technology. The electron source proposed for this scheme would be a field emitter array.[7] Another approach to this problem is that of scaling down a Hall thruster to much smaller dimensions than conventional systems.[8] Still another concept proposes the use of the hollow anode effect to generate a plasma in a high pressure cavity.[9] Finally, the use of a hollow cathode-based ion accelerator is also being investigated. In this concept, the hollow cathode orifice plasma provides the ions that feed a high voltage accelerator stage.[10,11] The future of these concepts hinge primarily on increasing the ionization

fraction within the discharge and reducing the complexity of the overall power processor.

The objective of the research presented here is to develop a simple, low power, compact plasma source that could be used stand-alone or as a plasma source that feeds a high voltage ion optics stage. The approach of this work utilizes a magnetic cusp to effectively utilize discharge electrons for ionization purposes and at the same time generate sufficiently high sheath potentials that accelerate ions, thereby generating a flowing plasma. This approach utilizes a single electron source that provides not only discharge electrons but also electrons to neutralize the ion beam generated. Additionally, the device is simplistic in design, making it quite rugged and straightforward to fabricate.

Conceptual Description of Compact Plasma Accelerator Concept

The general principle behind the operation of the compact plasma accelerator approach is outlined in Figure 1a. As illustrated in the Figure, propellant is injected through a plenum with capillary like openings so that even at low flow rates, the pressure in the plenum channels is sufficiently high (few Torr) such that the depth of the plenum channel openings (plenum tubing wall thickness) are of order an electron-neutral mean free path. The plenum, which is at anode potential, is centered above a magnetic cusp generated by a permanent magnet circuit comprised of a single ring of magnets and a center magnet. The cusp funnels energetic electrons into the plenum openings. These electrons ionize propellant inside the plenum channels. *The plasma production volume, as estimated from the depth of the orifice channel, is of order 1 mm.* Each plenum orifice serves as a *very compact*, independent discharge cell that provides copious amounts of ions that are subsequently accelerated by sheath potentials. An electron source, in this case a hot filament, provides the electrons. The annular electron source is located such that emitted electrons must undergo cross field-diffusion to reach the anode. Under this conditions, electron diffusion is severely restricted:[12]

$$\frac{D_\perp}{D_a} = \frac{1}{1 + \left(\dfrac{w}{\boldsymbol{n}}\right)^2} . \qquad (1)$$

The transverse magnetic field component tends to increase the cathode fall voltage. The increase in the cathode fall voltage is necessary to produce energetic electrons for ionization inside plenum channels. The maximum electron-neutral ionization cross section for xenon occurs around 150 eV. Cathode fall voltages of this order maximize ionization efficiency. Energetic electrons with a sufficient velocity component parallel to the magnetic field enter the orifice channel to participate in the ionization process. Those without sufficient parallel velocities are reflected by the mirror force:[13]

$$F_{\parallel} = -\boldsymbol{m} \frac{dB}{ds} \qquad (2)$$

Because the electrons reflected by the mirror force are constrained by the field lines, the reflected electrons will oscillate between the filament and the plenum. The likelihood that these electrons will ionize neutrals in the region of the plenum increases as energetic electrons bounce between the filament and the plenum. This motion enhances the primary electron residence time.

Ions formed in the plenum channel are accelerated by the potential gradient across the sheath at the plenum. The magnitude of the voltage drop at the anode is likely to be a strong function of the transverse field component there. The ions emitted from the sheath at the anode plenum form an axially directed beam. The ion beam is neutralized by electrons emitted into the beam by the filament. In this respect the filament not only provides the ionizing electrons but also the neutralizing electrons.

A hypothetical potential distribution for the device is shown in Figure 1b. Here cathode fall voltage at the filament extracts the electrons and provides them with sufficient energy to reach the anode, where they subsequently ionize gas at the orifice. The anode fall voltage accelerates these ions rearward, thereby generating the flowing plasma.

It should be pointed out that the choice of the electron source used in this device is quite general. In this study, a coated filament was used. The compact plasma accelerator (CPA) concept is also compatible with a field emitter array cathode. The appeal of this approach is the higher current density and simplicity of integration (no filament heater supply required).

Experimental Set-up

A laboratory model of the compact plasma accelerator is presented in Figure 2. The primary components include a gas plenum fabricated from non-magnetic, stainless steel tubing with a wall thickness of 0.74 mm. The tubing contains seven equally spaced, 0.18 mm diameter apertures. This gave an orifice channel aspect ratio of approximately 4. Each plenum opening is indicated by a number-label as shown in Figure 2. Pressure in each orifice at a given flow rate was estimated based on the volumetric flow and orifice diameter using the Poiseuille equation:[14]

$$Q = \frac{\boldsymbol{p} \cdot a^4}{8 \boldsymbol{h}_{\vdash}} \cdot P_a \cdot (P_2 - P_1) \qquad (3)$$

Poiseuille's equation applies in the viscous regime where the Knudsen number < 0.01. Because the flow rate $\boldsymbol{m}_T = Q/(P_2 - P_1)$, the pressure inside each orifice of the plenum can be directly related to the measured volumetric flow:

$$\boldsymbol{m}_T \Big/ N = \frac{\boldsymbol{p} \cdot a^4}{8 n_o \boldsymbol{h}_{\vdash}} \cdot P_a \qquad (4)$$

In this investigation, xenon was used as propellant. Xenon was chosen because of its low ionization potential (12 eV) and its high mass number 131 amu. For the flow rates (0.5-2.5 sccm) investigated in this work, the xenon pressure that develops in each aperture should range between 3 and 8 Torr. The mean free path at these pressures as a function of electron energy is shown in Figure 3. The mean free path is determined from the relation:

$$L = \frac{1}{\boldsymbol{s}_i \cdot n_o} \qquad (5)$$

As can be seen in the figure, the mean free path is of order the orifice channel dimensions over a wide electron energy range provided the pressure in the plenum is at least 0.75 Torr, a condition that is satisfied over all operating conditions investigated here. This assures ionization via collision to occur in the orifice over the energy range shown in Figure 3.

The electron source consisted of a double braided tantalum wire. The filament was coated with barium carbonate (R-500) to reduce its work-function so as to provide stable emission. During these tests, the filament temperature ranged between 1000 and 1040 C as measured using an optical pyrometer.

The magnetic circuit consisted of a single ring of samarium cobalt magnets located just under the plenum and a disk samarium cobalt magnet in the center of the device. The magnets' surface field strength was approximately 0.3 T. A mild steel plug, located on axis (see Figure 1a) was used to shape the magnetic field, primarily extending it outward to prevent the magnets from directly shorting (magnetic flux) to each other below the macor front plate. Figure 4 presents the calculated magnetic flux profile of the device. The cusps are clearly evident above the orifices of the plenum. Additionally, it is clear that electrons emitted from the cathode must undergo cross-field diffusion to reach the anode. Again, this effect increases the impedance of the discharge.

Experimental testing of this concept was performed in a 0.61 m diameter by 0.91 m long stainless steel bell jar with a 0.25 m cryo-pump. The cryo-pumped facility had a pumping speed of 4000 liters per second (nitrogen). The facility contained an automated data acquisition and control system, power console, and an integrated high-purity propellant feed system. Base pressure was approximately 10^{-7} Torr. During testing, operating pressure ranged between 3 x 10^{-5} Torr at 0.5 sccm to 7 x 10^{-5} Torr at 2.5 sccm of xenon.

Mounted within the vacuum facility was a 2D motion control system, with one stage capable of 408 mm of axial translation and a transverse stage capable of 208 mm of radial translation. Electrostatic probes were mounted atop the motion control system for plume interrogation. The probes used in this investigation were a Faraday probe and a retarding potential analyzer. The 3.2 mm diameter Faraday probe, biased –25 V with respect to ground to repel plasma electrons, was swept across the ion source to access the beamlet profile across aperture #1 of the compact plasma accelerator. Ion energies were measured using a simple two grid retarding potential analyzer. The entrance grid floated while the second grid was biased between 48 and 70 below ground to repel energetic electrons that happen to pass through the first floating grid. The collector plate, located downstream of the second grid, was biased positive relative to ground and served as both the collector and discriminating electrode. A schematic of the probe along with potential variations within the probe is shown in Figure 5. The ion energy distribution function can be obtained from the current-voltage characteristic of the retarding potential analyzer:[15]

$$f(u_i) = -\frac{M}{e^2 \cdot A} \cdot \frac{dI}{dV} \qquad (6)$$

Experimental Results

In order to assess the performance of the compact plasma accelerator as an ion source, a number of measurements were made: 1) I-V discharge characteristics measured as a function of flow rate 2) Ion current density profiles were measured at a fixed discharge current but at different flow rates 3) The ion energy distribution function was measured using a retarding potential analyzer 4) A Langmuir probe was used to measure downstream floating potential profiles.

Discharge Current-Voltage Characteristics

The compact plasma accelerator was operated over a discharge power range between 20 and 40 W (not including filament power (~10 W). Figure 6a illustrates typical current voltage characteristics of the compact plasma accelerator at different flow rates. The discharge current increases rather steeply with increases in discharge voltage. In this respect, the discharge can be characterized as only mildly resistive, with the discharge current increasing with increasing discharge voltage at a rate greater than linear. This behavior, is somewhat similar to hollow cathode plasma contactor clamping operation in that the source can provide a wide range of discharge current without a large change in voltage.[16] In most cases, for a given discharge current, the discharge voltage was higher at the lower flow rates. This behavior is attributed to primarily two processes: 1) Plasma impedance drops with increasing flow rate (orifice pressure) due to a higher electron-neutral collision frequency. 2) At the higher flow rates, electron diffusion across field lines is easier due to an increased collision frequency, thereby, reducing the voltage necessary to get electrons to the anode. Figure 6b also illustrates the sensitivity of the discharge to flow rate at a fixed discharge current. In this case, the discharge was operated at 98 mA. As can be seen in the Figure, the discharge voltage initially increases steeply with decreasing flow rate and then levels off somewhat at the lower flow rates. This behavior is attractive in that it suggests that operation at very low flow rates does not translate into large increases in discharge voltage.

Faraday Probe Data

In order to assess general characteristics of the ion beam produced as well as estimate the ionization efficiency of the CPA, downstream Faraday probe current density profile measurements were made. The current density measurements were acquired as a function of radial position across an individual beamlet diameter.

The data presented here was acquired at low flow rate operation < 1 sccm. Under these conditions, the discharge was present in only 4 (apertures 1,2 and 6,7) of the 7 apertures. (At higher flow rates, a discharge was present at all openings.) It is assumed that the current density profile across aperture #1 is similar to other "lit" apertures, which had comparable brightness. The absence of a discharge in apertures 3, 4, and 5 at the reduced flow rates is attributed to differences in orifice pressure, filament distance, and local magnetic field strength. The values of these parameters at the "unlit" apertures as compared to the "lit" apertures may not be favorable for adequate electron coupling to the gas to initiate and sustain a discharge. For this investigation, at these low flow rates sweeps were taken across aperture #1. The low flow rate sweeps across aperture #1 were taken approximately 14 mm downstream of the macor face-plate (approximately 24 mm downstream of the plenum itself).

Figure 7 shows variations in the current density profile taken by the Faraday probe taken across aperture #1 while the discharge operated at a 98 mA discharge current but at different flow rates (0.48 SCCM through 0.75 SCCM). A surprising aspect of the Faraday sweeps is that though spatially the peaks are roughly the same width, the peak current density increases dramatically with decreasing flow rate, suggesting optimization. This behavior suggests that the beam current increases with decreasing flow rate. Langmuir probe measurements taken farther downstream (34 mm) also show the ion saturation current increasing with decreasing flow rate. This behavior may be due in part to two effects: 1) At lower flow rates, the associated reduced gas pressure/density reduces the rate of ion-neutral scattering that would otherwise attenuate the ion flow. 2.) Reduced flow-rate/pressure tends to increase the total voltage and thus increase the ionization efficiency. Higher flow rates would reduce the average energy of the electrons (electron temperature) because of the associated smaller cathode

fall voltage and an increased electron-neutral collision frequency (electron cooling). At reduced flow rates, ion transport out of the device is more efficient. The higher ion currents at the reduced flow rates imply higher ionization fractions at the reduced flows. This behavior is similar to that observed in hollow cathodes, where the emitted ion current increases with decreasing flow rate.[11]

It was observed that the peak current density downstream of the aperture increases by two orders of magnitude as the flow is reduced from 0.75 to 0.48 sccm. At the 0.48 sccm flow rate, the peak current density (at the same downstream axial location) was measured to be approximately equal to that generated by 30 cm NSTAR-derivative ion thruster operating at 2.3 kW.[17] Accompanying this increase in ionization efficiency is an increase in discharge voltage, from 369 to 421V as flow is reduced from 0.75 SCCM to 0.48 SCCM. This increase in voltage is likely necessary to increase the ionization rate and thus sustain the 98 mA discharge.

The peaks in Figure 7 undergo a slight shift with decreasing flow rate. The peak shifts to left approximately 8 mm as the flow is reduced from 0.75 to 0.48 SCCM. This shift suggests that the centroid of the beam moves slightly off aperture-axis as the flow decreases (voltage increases). This may be due to focusing effects associated with the sheath at the anode or potentials at the exit plane of the front plate.

The rather abrupt drop off in current at the left side of the trace is most likely due to macor faceplate channels. The primary functions of the face plate were to channel the ion flow and to protect non-apertured anode surfaces from electron collection thereby forcing electron flow to the anode to occur only through the channels.

The beamlet generated at aperture 1 was integrated to estimate the ion current generated per aperture. Table I lists the integrated currents at the different flow rates. These numbers represent an estimate of the upper limit of ion current developed at aperture 1 since there may be some cross talk between the adjacent beamlets in the wings. The integrated current ranged from 0.6 to 7.5 mA as the flow was reduced from 0.75 SCCM to 0.48 SCCM. These modest beamlet currents indicate very high propellant utilization at very low flow rates and suggest high ionization fractions at the plenum

channels. Indeed, at 0.48 SCCM, the utilization was estimated to be approximately 88%. The high ion current densities and utilizations (between 5% and 88%) support the notion that this concept could be potentially useful as a low power, compact ion source.[11] The Table also lists the upper limit on the total ion beam current developed taking into account the sum of all the individual beamlets lit during the test (four in this case). It is assumed that each aperture generates the same ion beamlet. If all seven apertures were operating similarly, the total beam current would be approximately 1.75 times higher at each operating condition. In this case, higher flows rates might be required.

The ratio of ion current to discharge current is also high, ranging from 2% at 0.75 sccm to 30 % at 0.48 sccm. This parameter also suggests that discharge electron utilization is very good.

Ion energies

The retarding potential analyzer (RPA) was used to access the energy distribution of the ions making up the beamlet. For these measurements, the probe was located approximately 34 mm downstream of aperture #1. The discharge current was fixed at 98 mA while the flow rate was varied. The voltage on the retarding plate was then swept between 0 and 100 V. Figure 8 shows differentiated current voltage trace obtained from the RPA at 0.48 SCCM and 0.75 SCCM. The curves are area normalized. These curves indicate the ion energy distribution at the specified operating condition. As can be seen, the energy distribution is extremely peaked around 81 and 82 V respectively for the 0.75 SCCM and 0.48 SCCM cases. The width of these peaks is of order a few volts. In both flow rate cases, immediately to the left of the most prominent peak by approximately one volt, there is a smaller side lobe present. With the exception of the two small peaks near 69 V and 72 V in the 0.75 SCCM case, the ion energy distribution below 80 V is fairly flat. This data suggests that the ions emitted from the device consists primarily of a mono-energetic beam with an average value of approximately 81 eV at these low flow rates.

Coupled together with the Faraday analysis, the data suggests that the compact plasma accelerator, though un-optimized, is capable of generating a flowing plasma. The performance of this device as an ion source is best at the reduced flow rate of 0.48 SCCM.

At this condition the propellant utilization is highest. Based of the analyzed data, it is possible to make a rough estimate of the specific impulse and thrust of this device at this condition using the following performance equations:[18]

$$I_{sp} = \frac{\boldsymbol{h}_u \cdot \boldsymbol{g}}{g} \cdot \sqrt{\left(\frac{2 \cdot e \cdot V_b}{M}\right)} \qquad (7)$$

$$F = \boldsymbol{g} \cdot \sqrt{\left(\frac{2 \cdot M}{e}\right)} \cdot J_b \cdot \sqrt{V_b} \qquad (8)$$

Measurement of beam divergence losses was beyond the scope this work. For convenience, the thrust loss factor is neglected, thereby allowing an upper limit on the specific impulse and thrust developed at the 0.48 sccm operation condition to be computed. Using equations 7 and 8, the upper limits on the thrust and specific impulse are approximately 990 s and 0.5 mN respectively. There are some potential applications for the device operating at these conditions as a stand-alone thruster. For example, disturbance compensation missions typically require thrust in the micro-Newton to milli-Newton range. It should be pointed out that both the thrust and average ion energy can be increased by simple modifications. The thrust should increase with the number of active apertures. Additionally, increasing the transverse magnetic field component at the aperture should increase the anode sheath potential and therefore increase the average energy of the ejected ions.

Floating Potential Profiles

Floating potential measurements referenced with respect to tank ground were taken as a function of axial distance downstream of compact plasma accelerator. The floating potential of the Faraday probe was monitored as a function of axial position downstream of aperture #1. Assuming the electron temperature does not vary appreciably downstream of the device, the electric field can then be estimated from the negative gradient of the floating potential profile:

$$E \approx -\nabla V_f \qquad (9)$$

Figure 9a illustrates the variations in the floating potential as a function of axial distance downstream of the compact plasma accelerator. The zero axial location as defined here is the axial position of closest approach. This distance is approximately 14 mm downstream of the front- plate of the accelerator and

roughly 5 mm downstream of the plane of the filament. The floating potential plots can be approximated by exponential fits as shown in the Figure. From the fits a spatial decay constant can be obtained. The spatial decay constant increases with decreasing flow rate. This observation reflects the fact that the potential does not drop off as rapidly with increasing distance at lower flow rates. Plots of the electric field profile obtained by differentiating the floating potential according to Equation 9 are presented in Figure 9b. Here it can be observed that the electric field in the near field is fairly modest but as expected it decreases with increasing downstream axial position. The presence of a finite electric field indicates that the ion beam may not be completely neutralized at the distances indicated in the Figure. The reduction in the electric field with increasing axial distance, however, suggests that the degree of neutralization increases with increasing distance downstream of the thruster. The exponential decay constant for the electric field over the axial range interrogated increased with decreasing flow rate. This behavior suggest that relatively speaking, more neutralization takes place closer to the engine body at the low flow rates. The measured slowly varying electric field at the lower flow rates suggest that over the axial range interrogated, the measurements were made in the "tail" of the neutralization zone.

Conclusion

A compact plasma accelerator was designed and fabricated. Discharge characteristics of the compact plasma accelerator concept were measured. The discharge current variations with increasing discharge voltage were supra-linear. The device demonstrated the capability of generating ion beamlets (~80 eV) with downstream peak current densities comparable to that of higher power devices (7 mA/cm^2). In general, the device appeared to operate best at very low flow rates. High propellant utilization fractions were measured below 1 sccm (88% at 0.48 SCCM). Floating potential measurements made downstream of the device were used to estimate the downstream electric field. These measurements, which were used to qualitatively assess beam neutralization, indicated beam neutralization does occur downstream of the device. In conclusion, the CPA concept shows promise as a low energy ion source for propulsion applications or for low energy plasma/materials processing applications. Ion energies generated by the device are in the range required for thin film production and modification (for example, surface chemical modification).[19]

References

[1]Mueller, Juergen, "Thruster Options for Microspacecraft: A Review and Evaluation of Existing Hardware and Emerging Technologies," AIAA Paper 97-3058, 1997.

[2]Janson, S.W., "Chemical and Electric Micropropulsion Concepts for Nanosatellites," AIAA Paper 94-2998, 1994.

[3]Christensen, J.A., et al, " Design and Fabrication of a Flight Model 2.3 kW Ion Thruster for the Deep Space 1 Mission," AIAA Paper 98-3327, July 1998.

[4]Sovey, J.S., et al, "Development of an Ion Thruster and Power Processor for New Millenium's Deep Space 1 Mission," AIAA Paper 97-2778, December 1997.

[5]Mueller et al, "Micro-Fabricated Accelerator Grid System Feasibililty Assessment for Micro-Ion Engines," IEPC Paper 97-071, 1997.

[6]Brophy, J.R., "Micro-machined Ion Accelerators," NASA Tech. Briefs, 1996.

[7]Mueller, Juergen, Marrese, Colleen, Polk, Jay, and Wang, Joseph., "Design and Fabrication of a Micro-Ion Engine," AIAA Paper 2000-3264, 2000.

[8]Khayms, Vadim, and Martinez-Sanchez, M., "Preliminary Experimental Evaluation of a Miniaturized Hall Thruster," IEPC Paper 97-077, 1997.

[9]Young, Marc, Muntz, E.P., and Ketsdever, A.D., " Investigation of a Candidate Non-magnetic Ion Microthruster for Small Spacecraft Applications," AIAA Paper 98-3917, 1998.

[10]Katz, I., Davis, V.A., Mandell, M.J., and Patterson, M.J., " Hollow Cathode Micro-Thruster," AIAA Paper 2000-3267, 2000.

[11]Crofton, M.W., "The Feasibility of Hollow Cathode Ion Thrusters: A Preliminary Characterization," AIAA Paper 2000-5354, 2000.

[12]Chen, F.F., Introduction to Plasma Physics and Controlled Fusion, Plenum Press, New York, pp. 169-175, 1984.

[13]Chen, pp 30-34.

[14]Dushman, S., Scientific Foundations of Vacuum Technology, J. Wiley and Sons, NY, pp. 80-117, 1962.

[15]Hutchinson, I.H., Principles of Plasma Diagnostics, Cambridge University Press, pp. 79-84, 1987.

[16]Katz, I. et al, "Model of Plasma Contactor Performance," *Journal of Spacecraft and Rockets*, vol. 34, no. 6, Nov.-Dec. 1997, pp. 824-828.

[17]Foster, J.E., Soulas, G.C., and Patterson, M.J., "Plume and Discharge Plasma Measurements of an NSTAR-type Ion Thruster," AIAA Paper 2000-3812, 2000.

[18]Patterson, M.J., "Low-Isp Derated Ion Thruster Operation", AIAA Paper 92-3203, 1992.

[19]Grill, V. et al, "Collisions of ions with surfaces at chemically relevant energies: Instrumentation and phenomena," Rev. Sci. Instrum., vol. 72, no. 8, August 2001, pp. 3149-3179.

Table I.
Estimated Ion Beamlet Current Parameters

Flow Rate, SCCM	Discharge Voltage, V	Aperture 1 Beamlet Ion Current	Total Ion Beam Current (4 apertures)	Utilization (Beamlet current/Gas Flow in Eq. A)
0.48	421 V	7.5 mA	30 mA	0.88
0.60	376 V	1.3 mA	5.2 mA	0.12
0.75	369 V	0.6 mA	2.4 mA	0.05
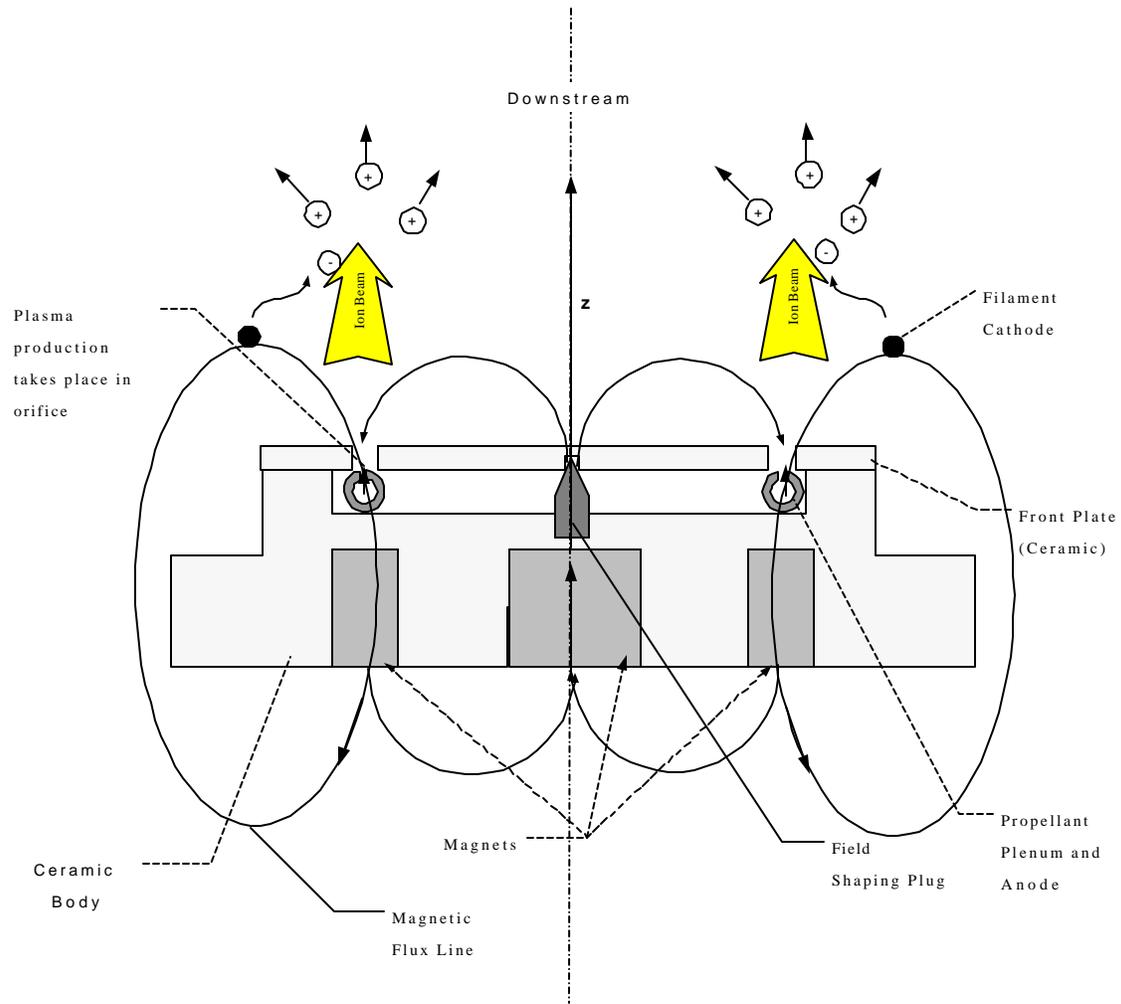
Figure 1a. Physical principles underlying the operation of the compact plasma accelerator. Device is cylindrically symmetric about z axis.
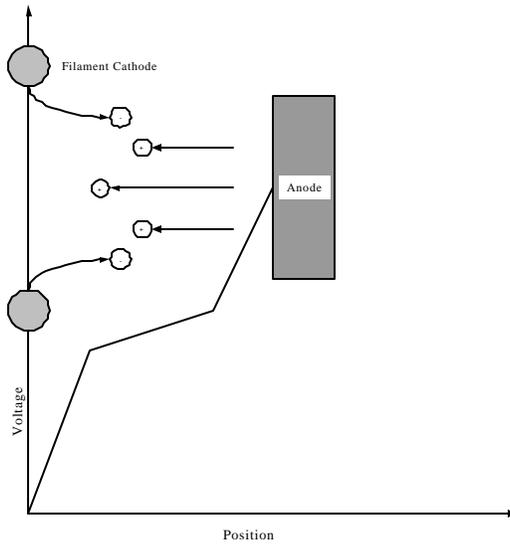
Figure 1b. Schematic of a hypothetical potential profile between filament cathode and anode.
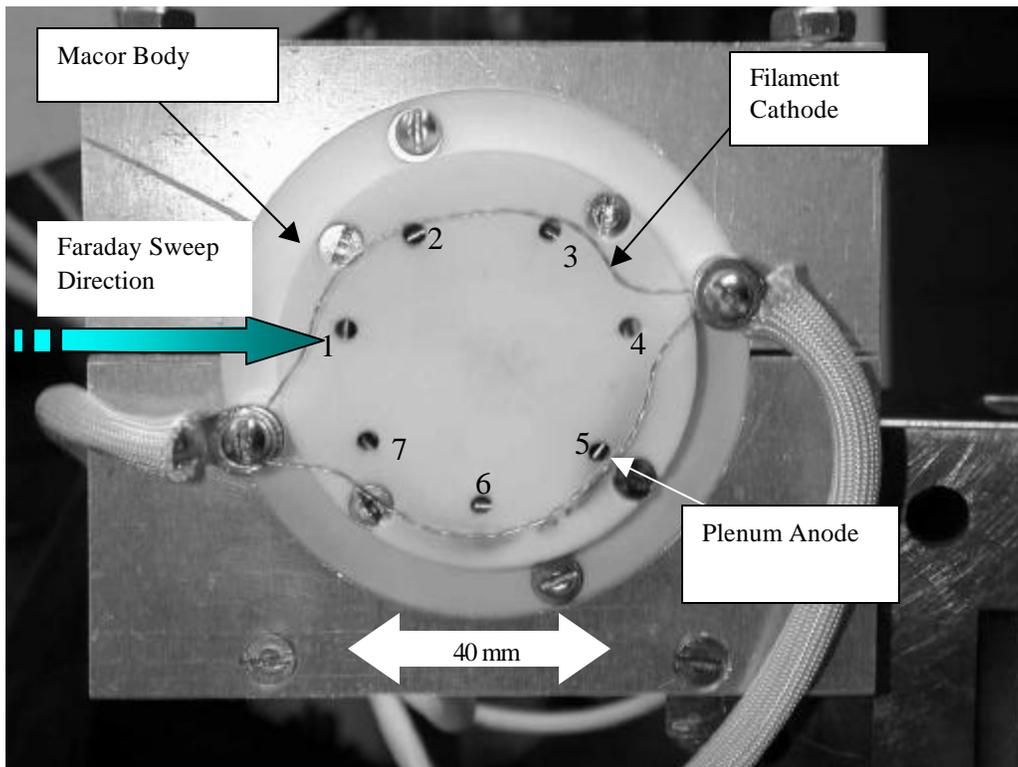
Figure 2. Compact Plasma Accelerator
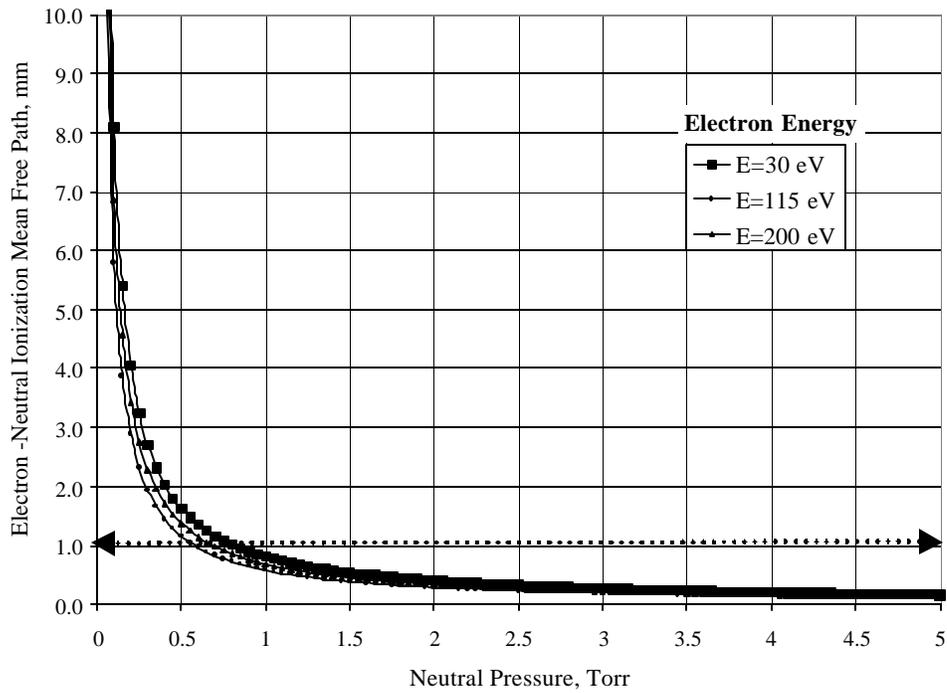
Figure 3. Ionization mean free paths as a function of pressure inside the orifice and electron energy.
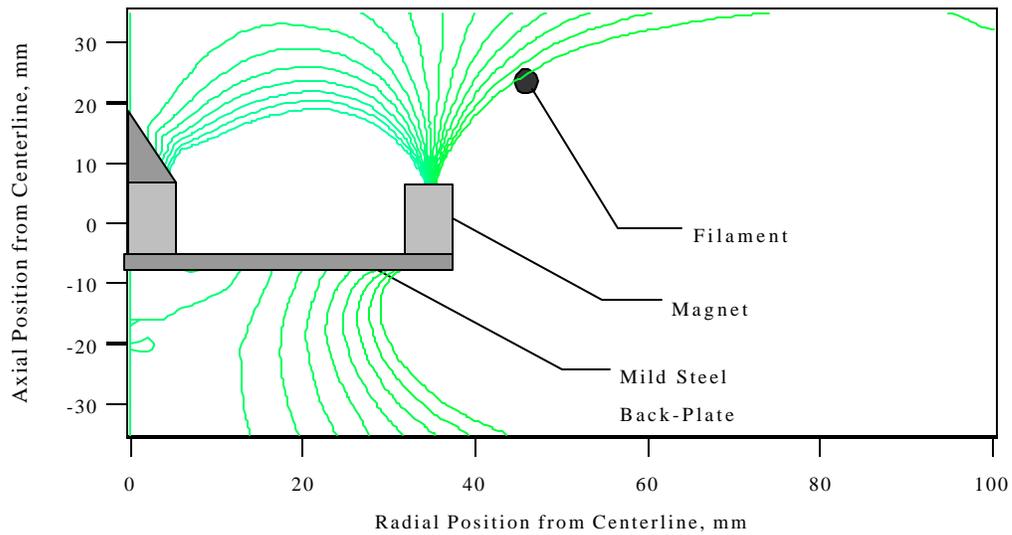
Figure. 4. Calculated magnetic flux contours of compact plasma accelerator (Half plane, cylindrically symmetric).
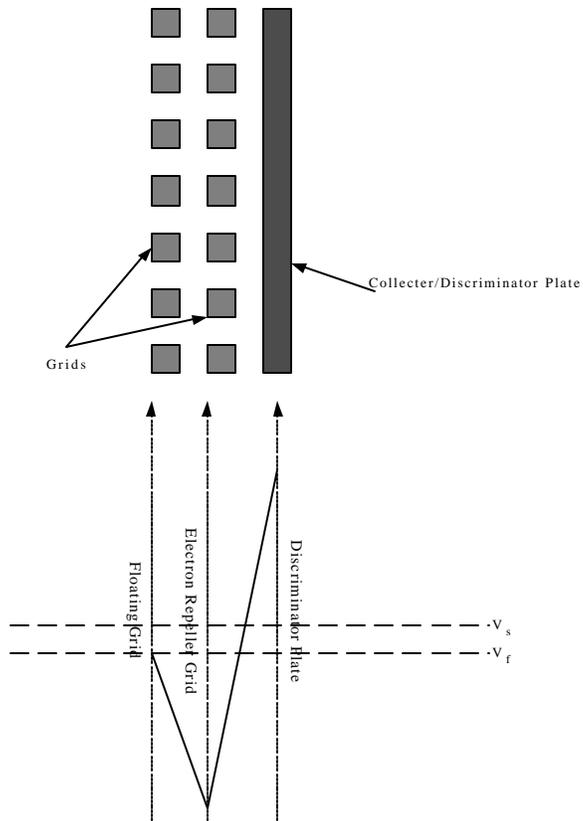
Figure 5. Retarding potential analyzer schematic.
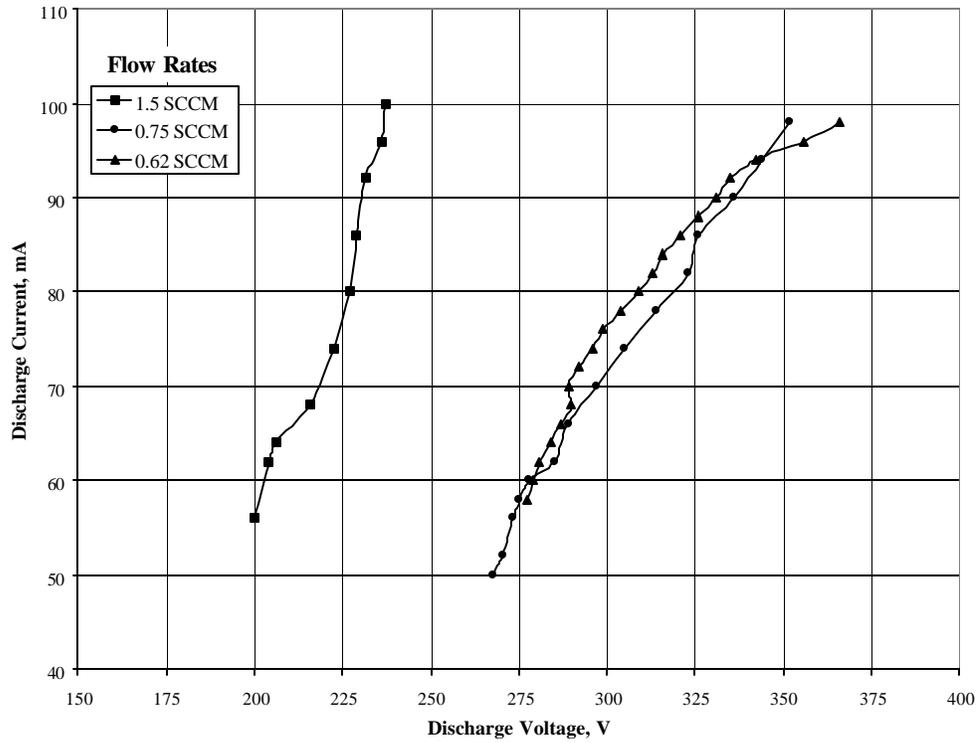
Figure 6a. Compact plasma accelerator discharge current-voltage characteristics at different xenon flow rates**.**
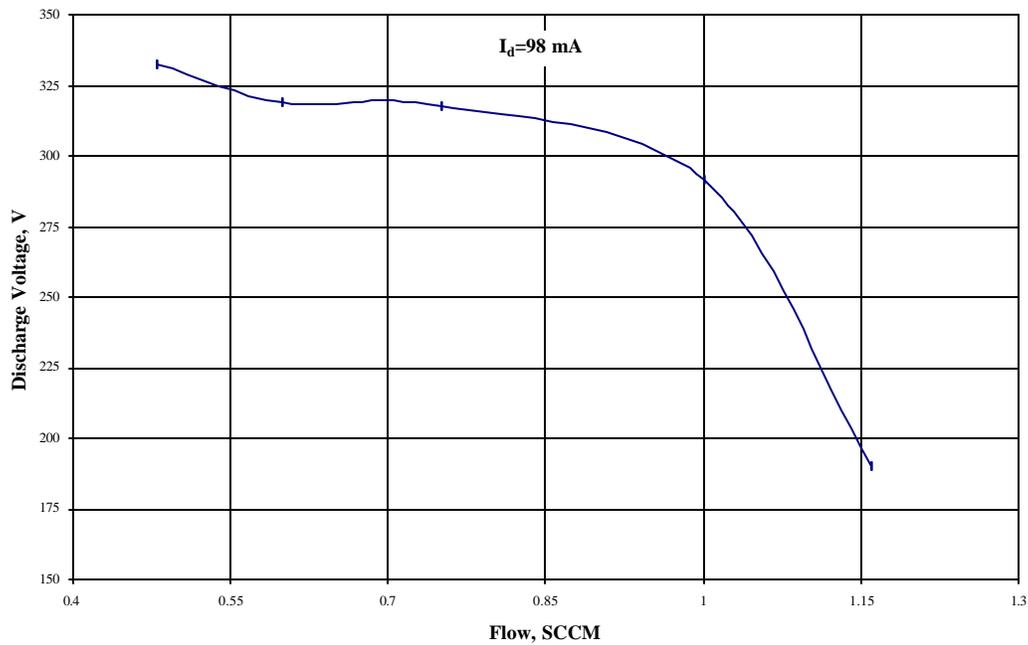
Figure 6b. Compact plasma accelerator discharge current-voltage characteristic variations with flow rate, at fixed discharge current.
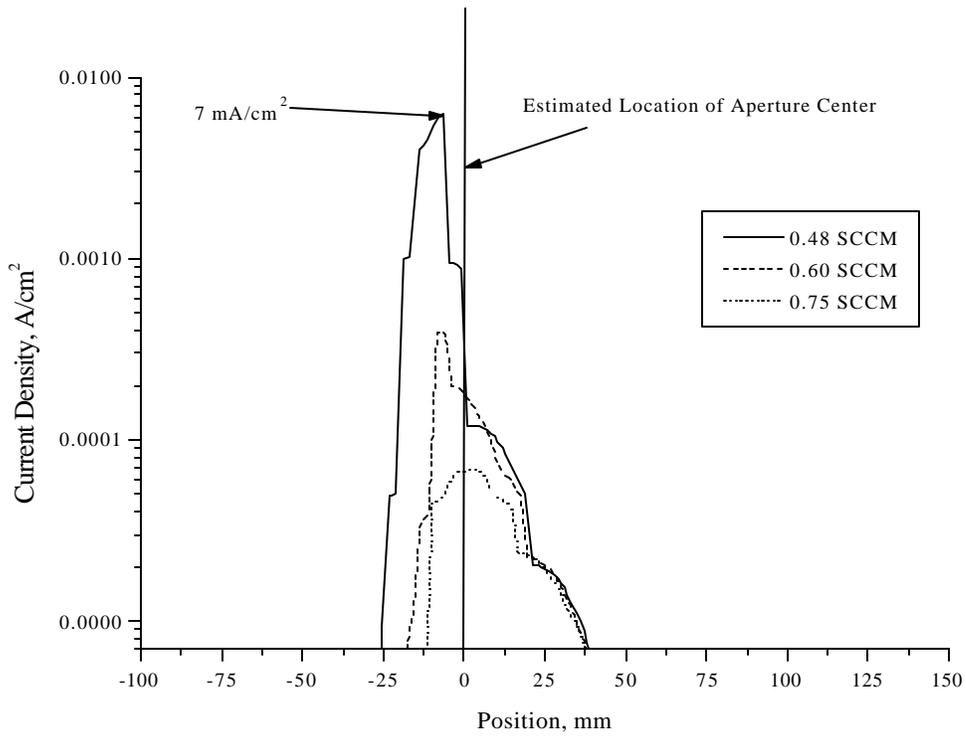
Figure 7. Variations in ion current density profiles downstream of aperture #1 as a function of flow rate.
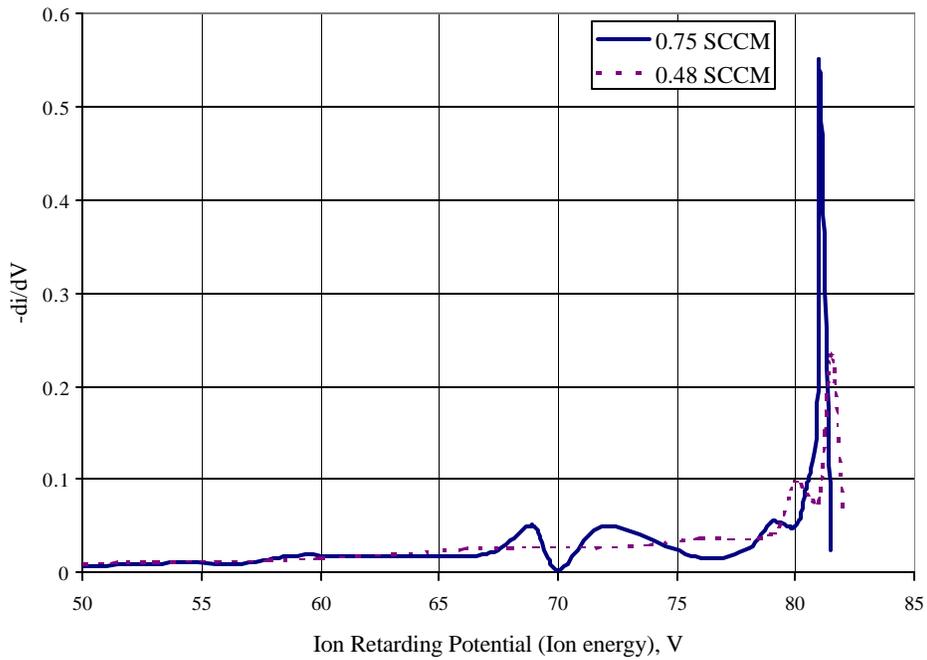
Figure 8. Ion energy distribution at different flow rates, I_d=98 mA.
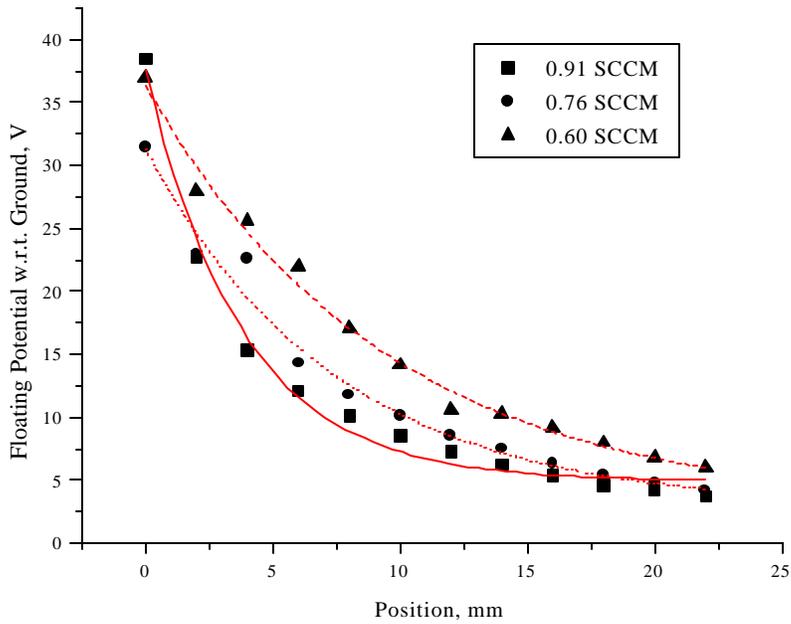
Figure 9a. Floating potential variations with increasing axial distance downstream of aperture #2 at different xenon flow rates. Note reference position z=0 is 14 mm downstream of the compact plasma accelerator faceplate.
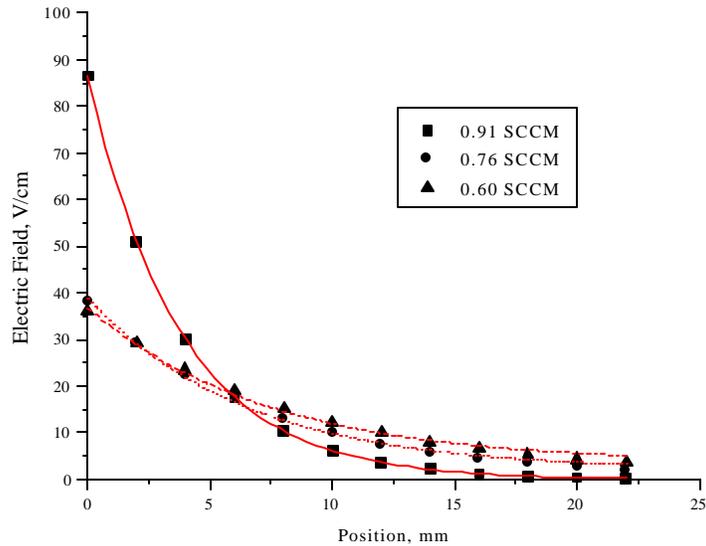
Figure 9b. Electric field variations with increasing axial distance downstream of aperture #2 at different xenon flow rates. Note reference position z=0 is 14 mm downstream of the compact plasma accelerator faceplate.